

# A novel FBG velocimeter with wind speed and temperature synchronous measurement

ZHU Xiu-bin (朱秀斌)\*

*School of Electric and Electronic Engineering, Zibo Vocational Institute, Zibo 255314, China*

(Received 7 March 2018; Revised 15 April 2018)

©Tianjin University of Technology and Springer-Verlag GmbH Germany, part of Springer Nature 2018

Based on frequency demodulation method, a novel fiber Bragg grating (FBG) velocimeter which can achieve wind speed and temperature synchronous measurement is proposed in this paper. The wind speed and temperature synchronous measurement is realized by cup anemometer (CA) signal modulation and Hilbert-Huang transformation (HHT) signal processing. The working principle of the novel FBG velocimeter is demonstrated and its theory calculation model is also set up by using basic mechanical knowledge and blade element momentum (BEM). Further, calibration experiment is carried out on one prototype of the FBG velocimeter to obtain its measurement performance. HHT is introduced to deal with calibration experiment data. After data analyses, the results show that the novel FBG velocimeter can achieve high-precision wind speed measurement of 0.012 m/s with minimum detection limit of 0.41 m/s, and its temperature detection precision is 10.6 pm/°C.

**Document code:** A **Article ID:** 1673-1905(2018)04-0276-4

**DOI** <https://doi.org/10.1007/s11801-018-8033-x>

Due to cost-related issue, dispatch planning and energy market operation, wind speed measurement is particularly important, especially in wind power generation industry<sup>[1]</sup>. Currently, the most commonly used wind speed measurement methods mainly include cup anemometer (CA)<sup>[2]</sup>, pitot tube anemometer (PTA)<sup>[3]</sup>, hot wire/film anemometer (HWA)<sup>[4]</sup>, acoustic doppler velocimeter (ADV)<sup>[5]</sup>, laser doppler velocimeter (LDV)<sup>[6]</sup>, particle image velocimeter (PIV)<sup>[7]</sup> and so on. However, harsh detection environment, such as high-low temperature and radioactive exposure, limits the application of these velocity detection methods. Due to its unique advantages, such as immunity to electromagnetic interference, compact size, resistance to corrosion, high sensitivity, long distance sensing and so on, several fiber Bragg grating (FBG) velocimeters have been reported<sup>[8-12]</sup>. All these FBG velocimeters are suitable for breeze measurement and have certain application limitations in outdoor operation, especially in large scale wind generation industry.

According to the above statement and the application environment of wind generation industry, a novel FBG velocimeter which can achieve synchronous measurement of wind speed and temperature is proposed in this paper. The FBG velocimeter is made up of the core sensitive element FBG, mechanical transition system, and protective shell. The mechanical transition system, which contains wind speed transfer element, strain modulation element and triangular cantilever beam, can achieve the modulation between wind speed and frequency of FBG center wavelength shift. Based on the basic mechanical knowledge and blade element momentum (BEM)<sup>[13,14]</sup>,

theory calculation model of the mechanical transition system is set up. Further, calibration experiment is also carried out on one prototype of the FBG velocimeter. To obtain detection environment temperature besides wind speed, HHT is introduced to deal with the experiment data. After experiment data analysis, wind speed and temperature detection accuracy of this FBG velocimeter are 84.91 Hz/(m/s) and 10.6 pm/°C, respectively. The results confirm that this FBG velocimeter can achieve wind speed and temperature synchronous measurement, and has practical application in wind generation industry.

The cutaway view and top view of the FBG velocimeter are shown in Fig.1. It is made up of the core sensitive element FBG, mechanical transition system, and protective shell. The mechanical transition system, which contains wind speed transfer element, strain modulation element and triangular cantilever beam, can achieve the frequency modulation between wind speed and FBG center wavelength shift. The working principle of the mechanical transition system can be explained as follows.

Step 1: According to the BEM theory, wind speed transfer element will be rotated by external wind speed.

Step 2: As the rotating force caused by wind speed transfer element is greater than the alternating resistance between strain modulation element and triangular cantilever beam, the strain modulation element will modulate the variation frequency of cantilever beam. When the rotating force equals the alternating resistance, the

\* E-mail: [zhuxiubin1976@126.com](mailto:zhuxiubin1976@126.com)

external wind speed is called the minimum detection limit of the FBG velocimeter.

Step 3: As strain modulation element and triangular cantilever beam are separated, the surface strain of the cantilever beam is changed regularly. The surface strain change leads to FBG wavelength shift.

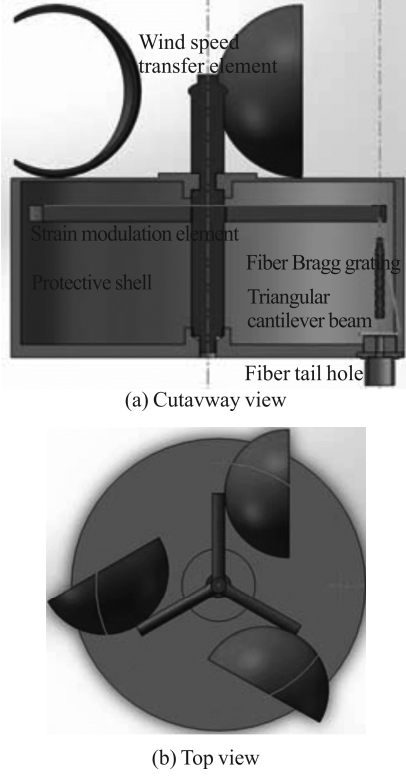


**Fig.1 Schematic of FBG velocimeter**

As the external wind continues, the mechanical transition system repeats from step 1 to 3. Then, HHT is utilized to obtain frequency and tendency signal of the wavelength shift of FBG. Further, wind speed and temperature can be obtained through the inversion of frequency and tendency signal.

Assuming that the external wind speed is  $V$ , the rotating force  $F$  on the wind speed transfer element can be expressed as

$$F = \rho S_{\text{eff}} (V - V')^2, \quad (1)$$

where  $\rho$  is the air density,  $V'$  is the wind speed after the velocimeter, and  $S_{\text{eff}}$  represents the effective area of the cup included in the wind transfer element as

$$S_{\text{eff}} = 2\pi r_c^2, \quad (2)$$

where  $r_c$  is the radius of the cup. Assuming that the interleaving length between strain modulation element and triangular cantilever beam is  $x$ , the alternating resistance  $F_a$  can be expressed as

$$F_a = \{Eh^3W[L^2 - (L-x)^2]^{1/2}\} / 6L^3, \quad (3)$$

where  $E$ ,  $L$ ,  $h$  and  $W$  are the elastic modulus, length, thickness and width at the fixed end of the cantilever beam, respectively.

As the rotating force  $F$  equals the alternating resistance  $F_a$  which means  $V'$  is zero, the minimum detection limit of the FBG velocimeter  $V_{\text{min}}$  can be expressed as

$$V_{\text{min}} = \{Eh^3W[L^2 - (L-x)^2]^{1/2} / 6\rho S_{\text{eff}}L^3\}^{1/2}. \quad (4)$$

The relationship between the rotating frequency of the strain modulation element  $f_m$  and the frequency of FBG wavelength shift  $f_i$  is

$$f_i = N f_m, \quad (5)$$

where  $N$  represents the number of teeth of the strain modulation element.

The wind speed transfer element and the strain modulation element are with coaxial connection. So, their rotating frequencies have the same value. Further, the measured wind speed  $V$  can be expressed as

$$V = R_c \cdot f_m / (2\pi), \quad (6)$$

where  $R_c$  represents the length between the center of the cup and the axis of the wind speed transfer element.

After HHT analyses, wavelength shifts of FBG  $\lambda_{\text{FBG}}$  can be expressed as

$$\lambda_{\text{FBG}} = \lambda_t + c_i, \quad i = 1, 2, \dots, n, \quad (7)$$

where  $\lambda_t$  and  $c_i$  stand for tendency signal and intrinsic mode function of the FBG wavelength shift signal. The tendency signal is utilized to obtain the testing environment temperature and their relationship can be expressed as<sup>[15]</sup>

$$(\lambda_t - \lambda_B) / \lambda_B = (\alpha + \zeta) \Delta T, \quad (8)$$

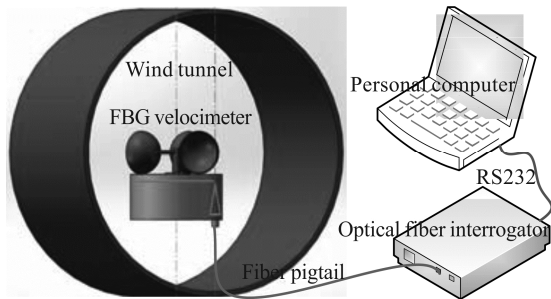
where  $\alpha$  is the thermal expansion coefficient,  $\zeta$  is thermo-optic coefficient of FBG,  $\lambda_B$  is initial center wavelength of FBG, and  $\Delta T$  represents the testing environment temperature variation.

To verify its measurement performance, one prototype of this FBG velocimeter is designed and manufactured. Main material of the protective shell is stainless steel. To reduce the influence of friction force caused by weights of wind speed transfer element and strain modulation element, their materials are both polyvinyl chloride. Based on its outstanding mechanical properties, low weight and corrosion resistance<sup>[16]</sup>, carbon fiber composite board is chosen as the material of triangular cantilever beam. The core sensitive element FBG is adhered on the front surface of the triangular cantilever beam. Basic geometrical parameters of this prototype are shown in Tab.1.

**Tab.1 Geometrical parameters of the FBG velocimeter prototype**

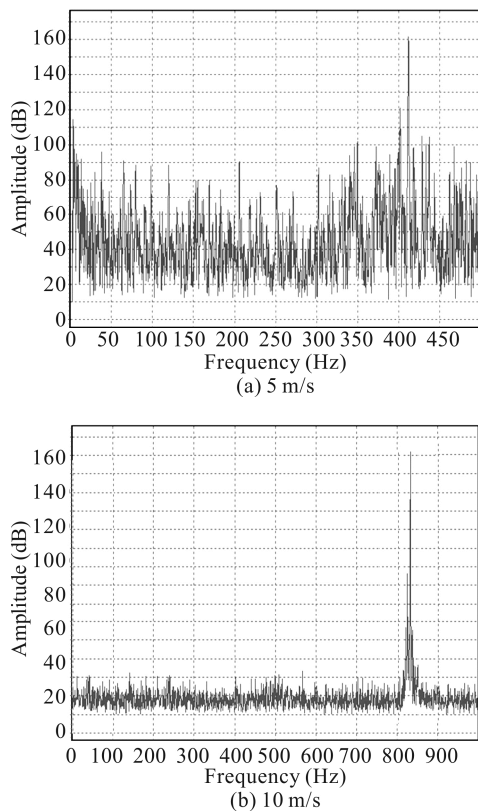
Symbol	Parameter	Value
$E$	Elasticity modulus	$1.65 \times 10^5$ MPa
$l$	Length of triangular cantilever beam	$15 \times 10^{-3}$ m
$W$	Width of fixed end	$10 \times 10^{-3}$ m
$h$	Height of triangular cantilever beam	$0.3 \times 10^{-3}$ m
$\rho$	Density of the air	$1.29$ kg/m <sup>3</sup>
$x$	Interleaving length	$0.5 \times 10^{-3}$ m
$r_c$	The radius of the cup	$15 \times 10^{-3}$ m
$N$	The number of teeth	60
$R_c$	Length between the center of the cup and the axis	$25 \times 10^{-3}$ m
$\lambda_B$	Initial center wavelength	1 545.956 9 nm

Fig.2 shows the schematic of the calibration experiment platform. Sense 20/20 (demodulation wavelength range 1 525—1 565 nm with precision of 1 pm) is chosen as the optical fiber interrogator in the platform. Its detection frequency range is 0—5 kHz and frequency demodulation precision is 1 Hz.



**Fig.2 Schematic of the calibration experiment platform**

At the beginning of the calibration experiment, the cup in the FBG velocimeter is kept still and personal computer acquires FBG center wavelength for almost 10 min. Mean value of the acquired data is chosen as the initial center wavelength  $\lambda_B$ . In the whole process of the calibration experiment, the airflow velocity in the wind tunnel is controlled to change in the range 0—15 m/s and the wind tunnel is placed in the room environment. Fig.3 shows the amplitude-frequency curves of the FBG wavelength signals corresponding to the airflow velocities of 5 m/s and 10 m/s.



**Fig.3 Calibration experiment data**

Signal to noise ratio (*SNR*) of the frequency amplitude curve of the FBG wavelength shift increases with the airflow velocity. Fig.4 shows the extracted frequency signal as a function of the airflow velocity.

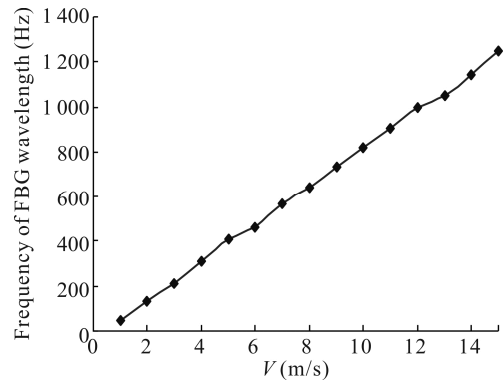


**Fig.4 Extracted frequency signal versus applied airflow velocity**

By using the least square method, the fitting curve between extracted frequency signal  $f_i$  and airflow velocity  $V$  can be expressed as

$$f_i = 84.91 f_m - 34.875, \quad R^2 = 0.92, \quad (9)$$

where  $R^2$  represents the linearity of the fitting curve. As its value is closer to 1, the linearity is better. According to the fitting curve, the wind speed detection sensitivity of the FBG velocimeter is 84.91 Hz/(m/s). So, its detection precision is 0.012 m/s due to the frequency demodulation precision of the fiber interrogator is 1 Hz. After calibration data analyses, the minimum detection limit of the FBG velocimeter is 0.41 m/s which is bigger than its theory calculation value 0.21 m/s. This phenomenon is mainly caused by the friction force between the wind speed transfer element and the protective shell. In conclusion, the FBG velocimeter can achieve high precision wind speed measurement with detection precision of 0.012 m/s and minimum detection limit of 0.41 m/s.

The airflow velocity in the wind tunnel is fixed at 5 m/s and the calibration experiment of testing environment temperature is carried out by changing the temperature of input airflow. In this experiment, the airflow temperature is changed from 20 °C to 50 °C with an interval of 5 °C. HHT<sup>[17]</sup> is introduced to extract tendency signal of the calibration experiment data and further obtain the testing environment temperature. The calibration experiment data corresponding to airflow temperature of 35 °C is chosen as the sample data to explain the HHT data processing, just as shown in Fig.5.

Tendency signal of the sample data only has a small decrease during the data sampling. This may be caused by the influence of the airflow velocity. After using the same data processing to analyze the experiment data and choosing the mean of tendency signal as the temperature corresponding data, Tab.2 shows the FBG wavelength

data with different external temperatures.

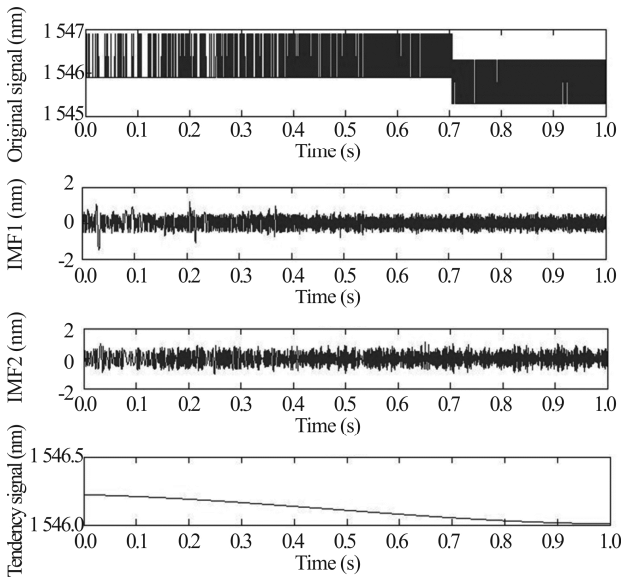


**Fig.5 Calibration experiment data processed by HHT**

**Tab.2 FBG wavelength data versus external temperature**

Temperature (°C)	FBG wavelength (nm)
20	1 545.791 5
25	1 545.846 9
30	1 545.902 4
35	1 545.957 9
40	1 546.014 4
45	1 546.068 9
50	1 546.115 4

The least square method is introduced to obtain the fitting curve between FBG wavelength  $\lambda_B$  and temperature  $T$ , which can be expressed as

$$\lambda_B = 0.0106 \cdot T + 1545.6, R^2 = 0.94. \quad (10)$$

Therefore, the measurement sensitivity of the testing environment temperature of the FBG velocimeter is 10.6 pm/°C with good linearity. Based on the above data

analyses, the FBG velocimeter proposed in this paper can achieve high-precision synchronous measurement of wind speed and environment temperature.

**References**

- [1] AM Foley, PG Leahy, A Marvuglia and EJ Mckeogh, *Renew. Energy* **37**, 1 (2012).
- [2] MA Baseer, JP Meyer, S Rehman, MM Alam and LM Al-Hadhrani, *Renew. Energy* **86**, 733 (2016).
- [3] Ryan B. Spelay, Kofi Freeman Adane and R. Sean Sanders, *Flow Measurement and Instrumentation* **45**, 247 (2015).
- [4] F. Mailly, A. Giani and R. Bonnot, *Sensors and Actuators A* **94**, 32 (2001).
- [5] Nicolas Gratiot, Mathieu Mory and Daniel Auchere, *Continental Shelf Research* **20**, 1551 (2000).
- [6] Koichi Maru and Kensaku Fujimoto, *Optik* **125**, 1625 (2014).
- [7] Qian Liao, Binbin Wang and Peifang Wang, *Flow Measurement and Instrumentation* **41**, 1 (2015).
- [8] L.J. Cashdollar and K.P. Chen, *IEEE Sens. J.* **5**, 1327 (2005).
- [9] X. Wang, X. Dong, Y. Zhou, K. Ni, J. Cheng and Z. Chen, *IEEE Photon. Technol. Lett.* **25**, 2458 (2013).
- [10] Xinhuai Wang, Xinyong Dong and Yan Zhou, *Sensors and Actuators A* **214**, 230 (2014).
- [11] M.A. Ibrar Jahan, Rajini V. Honnungar and R. Versha, *Materials Today: Proceedings* **5**, 302 (2018).
- [12] Wei Shen, Xiaoxing Wang, Lin Xu and Yingjiang Zhao, *Optik* **154**, 441 (2018).
- [13] R. Malki, A.J. Williams and T.N. Croft, *Applied Mathematical Modelling* **37**, 3006 (2013).
- [14] Rami Malki, Ian Master and Alison J. Williams, *Renew. Energy* **63**, 46 (2014).
- [15] Y.X. Guo, D.S. Zhang, Z.D. Zhou, L.T. Li and F.D. Zhu, *Journal of Optoelectronics-Laser* **25**, 435 (2014). (in Chinese)
- [16] Weidong Nie, Jie Llu, Wenbin Llu, Jun Wang and Tao Tang, *Polymer Degradation and Stability* **111**, 247 (2015).
- [17] Mingzhou Liu, Jiangxin Yang, Yanpeng Cao, Weinan Fu and Yanlong Cao, *Mechanical Systems and Signal Processing* **86**,177 (2017).